

# Renal Deletion of LRRC8/VRAC Channels Induces Proximal Tubulopathy

Karen I. López-Cayuqueo <sup>1</sup>, Rosa Planells-Cases <sup>1</sup>, Matthias Pietzke,<sup>2</sup> Anna Oliveras,<sup>1</sup> Stefan Kempa,<sup>2</sup> Sebastian Bachmann,<sup>3</sup> and Thomas J. Jentsch <sup>1,4</sup>

<sup>1</sup> Leibniz-Forschungsinstitut für Molekulare Pharmakologie (FMP) and Max-Delbrück-Centrum für Molekulare Medizin (MDC), Berlin, Germany

<sup>2</sup> Integrative Metabolomics and Proteomics, Berlin Institute of Medical Systems Biology/Max-Delbrück-Centrum für Molekulare Medizin, Berlin, Germany

<sup>3</sup> Department of Anatomy, Charité Universitätsmedizin Berlin, Berlin, Germany

<sup>4</sup> NeuroCure Centre of Excellence, Charité Universitätsmedizin Berlin, Berlin, Germany

## ABSTRACT

**Background** Volume-regulated anion channels (VRACs) are heterohexamers of LRRC8A with LRRC8B, -C, -D, or -E in various combinations. Depending on the subunit composition, these swelling-activated channels conduct chloride, amino acids, organic osmolytes, and drugs. Despite VRACs' role in cell volume regulation, and large osmolarity changes in the kidney, neither the localization nor the function of VRACs in the kidney is known.

**Methods** Mice expressing epitope-tagged LRRC8 subunits were used to determine the renal localization of all VRAC subunits. Mice carrying constitutive deletions of *Lrrc8b–e*, or with inducible or cell-specific ablation of *Lrrc8a*, were analyzed to assess renal functions of VRACs. Analysis included histology, urine and serum parameters in different diuresis states, and metabolomics.

**Results** The kidney expresses all five VRAC subunits with strikingly distinct localization. Whereas LRRC8C is exclusively found in vascular endothelium, all other subunits are found in the nephron. LRRC8E is specific for intercalated cells, whereas LRRC8A, LRRC8B, and LRRC8D are prominent in basolateral membranes of proximal tubules. Conditional deletion of LRRC8A in proximal but not distal tubules and constitutive deletion of LRRC8D cause proximal tubular injury, increased diuresis, and mild Fanconi-like symptoms.

**Conclusions** VRAC/LRRC8 channels are crucial for the function and integrity of proximal tubules, but not for more distal nephron segments despite their larger need for volume regulation. LRRC8A/D channels may be required for the basolateral exit of many organic compounds, including cellular metabolites, in proximal tubules. Proximal tubular injury likely results from combined accumulation of several transported molecules in the absence of VRAC channels.

JASN 33: 1528–1545, 2022. doi: <https://doi.org/10.1681/ASN.2021111458>

Animal cells have flexible, water-permeable outer membranes that cause cells to shrink or swell when exposed to osmotic gradients. Extracellular osmolarity is tightly controlled in most mammalian tissues, but can fluctuate widely in organs such as the kidney.<sup>1–3</sup> Hence cell volume regulation, which counteracts osmotic shrinkage or swelling, is highly relevant for renal cells. Cell volume regulation is not only crucial for preventing cell bursting with strong extracellular hypotonicity, but for keeping cytoplasmic concentrations of

Received November 11, 2021. Accepted May 13, 2022.

Published online ahead of print. Publication date available at [www.jasn.org](http://www.jasn.org).

See related editorial, “Unfulfilled Expectations Open New Horizons: What Have We Learned about Volume-Regulated Anion Channels in the Kidney?” on pages 1437–1439.

**Correspondence:** Dr. Thomas J. Jentsch or Dr. Rosa Planells-Cases, Leibniz-Forschungsinstitut für Molekulare Pharmakologie and Max-Delbrück-Centrum für Molekulare Medizin, Robert-Rössle-Straße 10, 13125 Berlin, Germany. Email: [jentsch@fmp-berlin.de](mailto:jentsch@fmp-berlin.de) or [planells-cases@fmp-berlin.de](mailto:planells-cases@fmp-berlin.de)

Copyright © 2022 by the American Society of Nephrology

proteins and second messengers in a narrow range.<sup>4–6</sup> Cell volume regulation relies on plasma membrane transport of osmoticants which reduces and finally inverts osmotic gradients that have caused cell volume changes in the first place.

Osmoticants include ions (mainly  $K^+$ ,  $Cl^-$ , and  $Na^+$ ) and various metabolites such as taurine, *myo*-inositol, and glutamate. Acute regulatory volume decrease (RVD) after cell swelling relies on the cellular loss of  $K^+$  and  $Cl^-$ , both through electrically coupled  $K^+$  and  $Cl^-$  channels and electroneutral  $K^+Cl^-$  cotransporters, or the efflux of organic osmoticants.<sup>4–6</sup> The latter efflux occurs largely through volume-regulated anion channels (VRACs), which also mediate swelling-induced  $Cl^-$  efflux. Acute regulatory volume increase, by contrast, involves uptake of  $Na^+$  and  $Cl^-$ . It occurs either through  $Na^+K^+2Cl^-$  cotransporters, or through indirectly coupled  $Na^+/H^+$  and  $Cl^-/HCO^-$  exchangers. Almost all ion transporters involved in cell volume regulation have additional functions such as regulation of intracellular pH or transepithelial transport.<sup>4,6</sup>

In the kidney, attention has been focused on cell volume regulation in the medulla that can experience very high osmolarity changes. Although acute regulatory volume increase involves ion transport processes described above, the increased cytosolic amounts of  $Na^+$  and  $Cl^-$  are later replaced by “inert” organic osmoticants to maintain crucial plasma membrane ion gradients.<sup>2,4,6</sup> These osmolytes include sorbitol, betaine, taurine, and *myo*-inositol.<sup>7–9</sup> They may be newly synthesized<sup>10</sup> or taken up by  $Na^+$ -coupled transporters.<sup>11–13</sup> Upon subsequent RVD, they may leave cells through VRACs.

Less attention has been paid to cell volume regulation in other nephron segments. Mice lacking basolateral  $K^+Cl^-$  cotransporters KCC3 and KCC4 displayed impaired RVD in proximal tubules (PTs).<sup>14</sup> In cultured PT cells, RVD was described to depend on basolateral TASK2  $K^+$  channels and VRACs.<sup>15,16</sup> Not surprisingly, typical  $I_{Cl,vol}$  volume-activated VRAC currents were detected also in other renal epithelial cells.<sup>17,18</sup>

VRACs are ubiquitously expressed in vertebrates and mediate RVD in many cells types.<sup>4,5,19</sup> Surprisingly, almost nothing is known on their role in the kidney. This dearth of information stems from the only recent identification of VRACs as heteromers of LRRC8 proteins.<sup>20</sup> VRACs require LRRC8A as an essential subunit,<sup>20,21</sup> but need at least one other LRRC8 isoform (LRRC8B–E) to form functional channels.<sup>20</sup> LRRC8 proteins assemble to hexamers.<sup>22,23</sup> Differently composed VRACs display distinct biophysical properties<sup>20,24</sup> and substrate specificities.<sup>25,26</sup> For instance, inclusion of LRRC8D greatly increases VRACs’ permeability to taurine, amino acids, *myo*-inositol, and drugs such as cisplatin.<sup>25,26</sup> VRACs’ role in cisplatin resistance<sup>26</sup> and the transport of the immunomodulator cGAMP<sup>27,28</sup> suggest biologically significant transport activity even under isotonic conditions.

### Significance Statement

Kidney cells are exposed to large changes in osmolarity and hence require efficient volume regulation. Volume-regulated anion channels (VRACs) mediate regulatory volume decrease, but their expression and function in the kidney remain enigmatic. VRACs, heterohexamers of LRRC8 proteins, also conduct metabolites. This paper describes the renal expression pattern of all five LRRC8 subunits and explores their roles in mouse models. Except for vasculature-restricted LRRC8C, all LRRC8 proteins are found along the nephron. Rather than in medulla, which experiences large osmolarity changes, VRACs are most highly expressed in proximal tubules, which have metabolite-conducting LRRC8A/D channels. Targeted disruption of either subunit injures the proximal tubule and produces Fanconi-like symptoms. VRACs may mediate nonspecific exit of organic compounds in this highly transporting nephron segment.

Capitalizing on several new genetic mouse models, we now show that VRAC subunits display highly distinct renal expression patterns. Whereas LRRC8A was found in virtually all cells, LRRC8C appeared restricted to vascular endothelial cells. In addition to LRRC8A, LRRC8B and LRRC8D were markedly expressed in basolateral membranes of PTs and to a lesser degree in more distal nephron segments. LRRC8E appeared specific for intercalated cells (ICs). Disruption of either LRRC8A or LRRC8D resulted in structural damage of the PTs and in functional abnormalities such as increased diuresis and Fanconi-like symptoms including mild proteinuria and glycosuria. We conclude that metabolite-conducting LRRC8A/D channels are crucial for PT function.

## METHODS

### Mice

All animal experiments were approved by and performed in compliance with local authorities (LAGeSo Berlin, Germany). Mice were housed under standard conditions in the Max-Delbrück-Centrum für Molekulare Medizin (MDC) animal facility according to institutional guidelines. Experiments were performed in 10- to 14-week-old male and female mice.

The generation of the conditional *Lrrc8a*<sup>lox/lox</sup> mice, the conditional knockin *Lrrc8a*<sup>HAlox/HAlox</sup> mice, and the conditional *Lrrc8d*<sup>Td1lox/Td1lox</sup> mice were described elsewhere.<sup>29,30</sup> Knockin mice carrying an epitope tag sequence fused at the C-terminal end of LRRC8B, LRRC8C, or LRRC8E were newly generated by CRISPR-Cas9 technology by the Transgenic Core Facility (TCF) at the MDC (TCF-MDC) (Berlin, Germany). smFPMMyc<sup>31</sup> (GFP variant containing several Myc-epitopes) was fused to *Lrrc8b* yielding *Lrrc8b*<sup>smFPMMyclox/smFPMMyclox</sup> mice, a double V5 sequence was fused to *Lrrc8c* in *Lrrc8c*<sup>V5/V5</sup> mice, and smFPV5<sup>31</sup> (containing several V5 epitopes) was attached to *Lrrc8e* in *Lrrc8e*<sup>smFPV5/smFPV5</sup> mice.

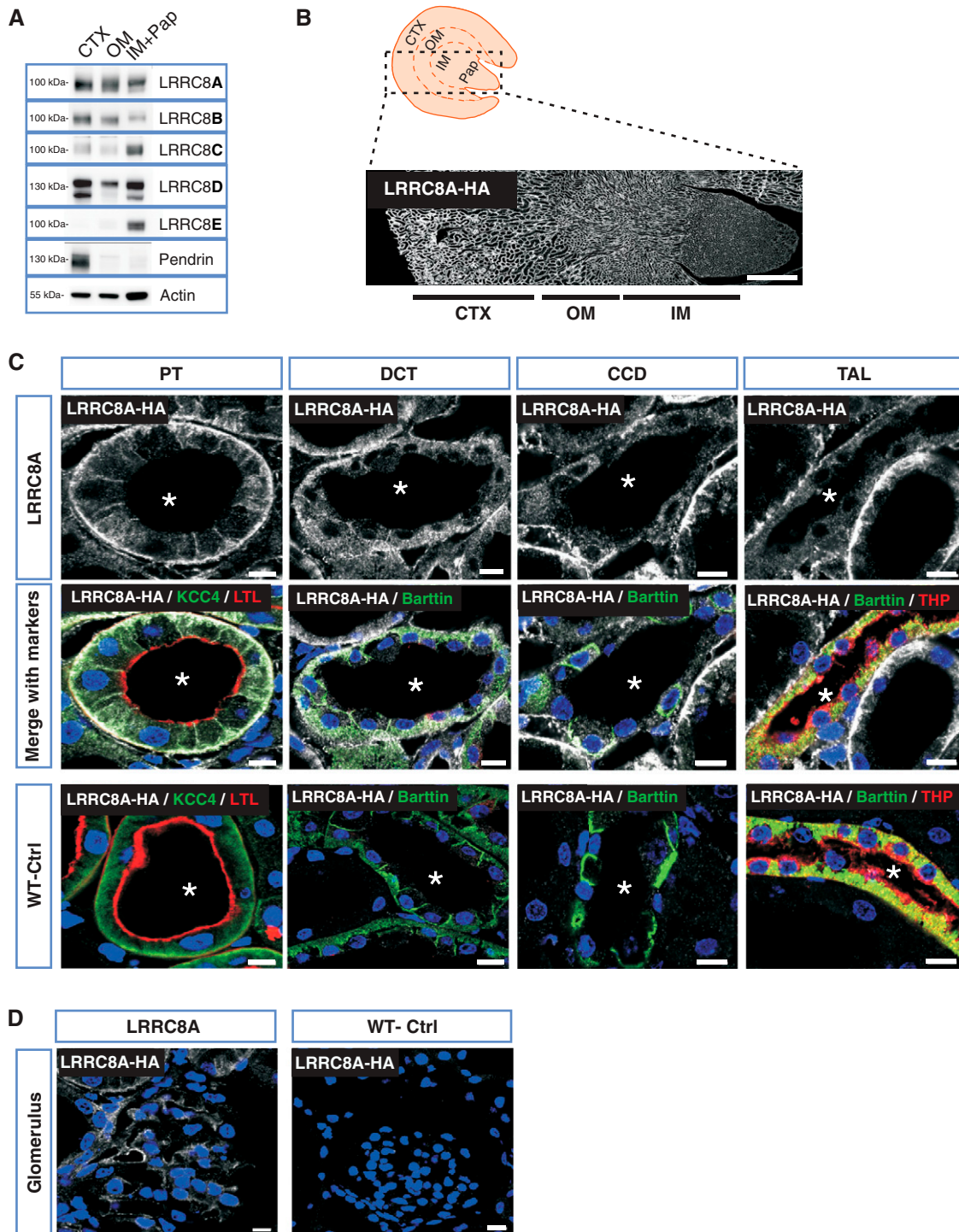


**Figure 1. Renal localization of the mandatory VRAC subunit LRRC8A.** (A) Representative Western blot analysis of the five VRAC subunits (LRRC8A–E) in membrane fractions isolated from different kidney regions: cortex (CTX), outer medulla (OM), inner medulla (IM), and papilla (Pap) from WT mice. Pendrin served as CTX marker and  $\beta$ -actin as loading control (shown as example for pendrin gel). Samples from CTX and OM were pooled from two mice, whereas IM+Pap were combined from six mice. (B) Panoramic view of LRRC8A-HA expression in *Lrrc8a*<sup>HAlox/HAlox</sup> kidney, using an HA antibody (white). Approximate localization of cortex, outer medulla, and inner medulla are indicated below. (C) Immunodetection of HA-tagged LRRC8A (white) in different renal tubule segments. PT was identified with luminal labeling with *Lotus tetragonolobus* Lectin (LTL) (red) and KCC4 (green) at the basolateral membrane. DCT was recognized by the basolateral staining of Barttin (green), which also expresses in ICs of CCD and TAL. TAL was additionally

**Figure 1.** (Continued) labeled with Tamm–Horsfall protein (THP) (red) at the apical membrane. The lumen of tubules is indicated by an asterisk. (D) Expression of LRRC8A-HA in glomerulus (white). Antibody specificity was tested in WT mice (WT-Ctrl). Nuclei stained with DAPI (blue). Scale bars, 10  $\mu\text{m}$  (DCT, PT, glomerulus), 5  $\mu\text{m}$  (CCD, TAL), and 500  $\mu\text{m}$  (whole kidney). Representative pictures of three mice per genotype.

*Lrrc8d*<sup>-/-</sup> mice were generated by CRISPR-Cas9 at the TCF-MDC. *Lrrc8d*<sup>-/-</sup> mice carried a 14-bp deletion (nucleotides 43–56) in the coding sequence, resulting in an early stop codon before the first transmembrane domain.

*Lrrc8b*<sup>-/-</sup> mice were generated using targeted embryonic stem cells (*Lrrc8btm1a*(KOMP)) obtained from the European Conditional Mouse Mutagenesis Program (EuCOMM). *Lrrc8c*<sup>-/-</sup> mice were produced using sperm donated by I. Masayoshi (Nagoya City University) via RIKEN. *Lrrc8e*<sup>-/-</sup> mice were produced by CRISPR-Cas9 at the TCF-MDC and have already been reported.<sup>27</sup>

For conditional deletion of *Lrrc8a*, *Lrrc8a*<sup>lox/lox</sup> mice were crossed with the following Cre-lines: ApoE-Cre,<sup>32</sup> Villin-Cre,<sup>33</sup> Ksp-Cre,<sup>34,35</sup> and Tie2-Cre.<sup>36</sup> Inducible nephron-specific *Lrrc8a* knockout (KO) mice were generated using *Lrrc8a*<sup>lox/lox</sup> mice additionally expressing Pax8-rtTA and Tet-On LC-1.<sup>37</sup> The 8- to 12-week-old *Lrrc8a*<sup>lox/lox</sup>/*Pax8*<sup>+</sup>/*LC1*<sup>+</sup> male/female mice were fed with doxycycline-containing food (6 g doxycycline/kg) for 2 weeks. Mice were used 3–7 days after discontinuing doxycycline treatment, unless otherwise specified. Doxycycline-induced *Lrrc8a*<sup>lox/lox</sup>/*Pax8*<sup>-</sup>/*LC1*<sup>-</sup> littermates were used as control mice.

### Blood and Urine Analysis

Mice were anesthetized with ketamine and xylazine intraperitoneally. For electrolyte and pH analyses (using iSTAT handheld blood analyzer with EC8+ cartridges, Abbott Laboratories), blood was collected by retrobulbar puncture using Na<sup>+</sup>-heparin capillaries. Blood osmolarity was calculated using the following equation:  $2 \times [\text{Na}^+] + [\text{urea}] + [\text{glucose}]$  (blood concentrations in millimolars).<sup>38</sup> For serum creatinine and copeptin determination, blood was collected from the beating heart of anesthetized mice. After 20 minutes at room temperature, the blood was centrifuged at 2000g to obtain serum in the supernatant. Creatinine was measured by enzymatic assay at the MDC Animal Phenotyping Facility and copeptin determination was by ELISA kit (Cloud-Clone Corp, #CEA365Mu).

Mice were singly housed in metabolic cages (Uno BV, Netherlands) for 2 days with free access to water (adaptation period) before urine was collected under water-saturated mineral oil for 24 hours. Mice were then water-deprived for 24 hours. Urine was collected every few hours to prevent food and fecal contamination. Urine electrolytes were analyzed at the MDC Animal Phenotyping Facility and urine pH by using a microelectrode (Mettler Toledo, #10333243).

### Antibodies

Polyclonal antibodies against the individual LRRC8 subunits were raised in rabbits (Pineda-Antikörper-Service,

Germany) and their specificity was ascertained using KO controls<sup>20,25,26,29,30</sup> (Supplemental Figure 1A). LRRC8A-HA protein was detected with anti-HA antibodies (Cell Signaling Technology, #3724 or Roche, #11867423001), LRRC8D-TdTomato was detected with an anti-RFP antibody (Rockland, #600401379), LRRC8B-smFPMyc was detected with Myc antibody (ChromoTek, #9e1-100), and both LRRC8C-V5 and LRRC8E-smFPV5 were detected with a V5 antibody (Biozol, #orb256446). Other antibodies used are listed in Supplemental Table 1.

Secondary antibodies were from Molecular Probes (coupled to Alexa 488, Alexa 555, or Alexa 633) or from Jackson ImmunoResearch (coupled to horseradish peroxidase). DAPI was from Invitrogen and *Lotus tetragonolobus* Lectin LTL (Fluorescein FL-1321) from Vector Laboratories.

### Western Blot Analysis

Membrane homogenates from whole kidney or kidney regions were quantified by BCA assay. Equal amounts of protein were separated by SDS-PAGE and blotted onto nitrocellulose membranes which were probed with the indicated antibodies (Supplemental Table 1) and detected by luminescence (SuperSignal, Thermo Fisher Scientific, #34580). ImageJ was used for quantification of the Western blots. Protein levels were normalized to actin controls on the same blot.

### Histology and Immunofluorescence

For histology, mice were perfused with 4% PFA/PBS. Next, 4- $\mu\text{m}$  paraffin-embedded tissue sections were stained with Masson's trichrome (Dianova, TRM-1), periodic acid-Schiff (Merck, HX961795), or hematoxylin (Sigma, #1092490500)/eosin (Roth, #CI45380). Images were acquired with an Axio-phot microscope. For immunofluorescence, mice were perfused with 1% PFA/PBS and kidneys frozen in cold isopentane. Next, 4- $\mu\text{m}$  sections were treated with 0.25% Triton X-100, blocked with 1% BSA, and incubated overnight at 4°C with primary antibodies (Supplemental Table 1) and later with secondary antibodies and counterstained with DAPI (Invitrogen). Confocal images were acquired with a Zeiss LSM880 confocal laser scanning microscope.

### Transdermal Measurement of GFR

GFR was determined according to Scarfe *et al.*<sup>39</sup> Transdermally determined FITC-sinistrin fluorescence decay was converted into GFR as described.<sup>40</sup>

### Statistical Analyses

Data are shown as mean  $\pm$  SEM, where *n* represents the number of animals. Statistical significance between groups

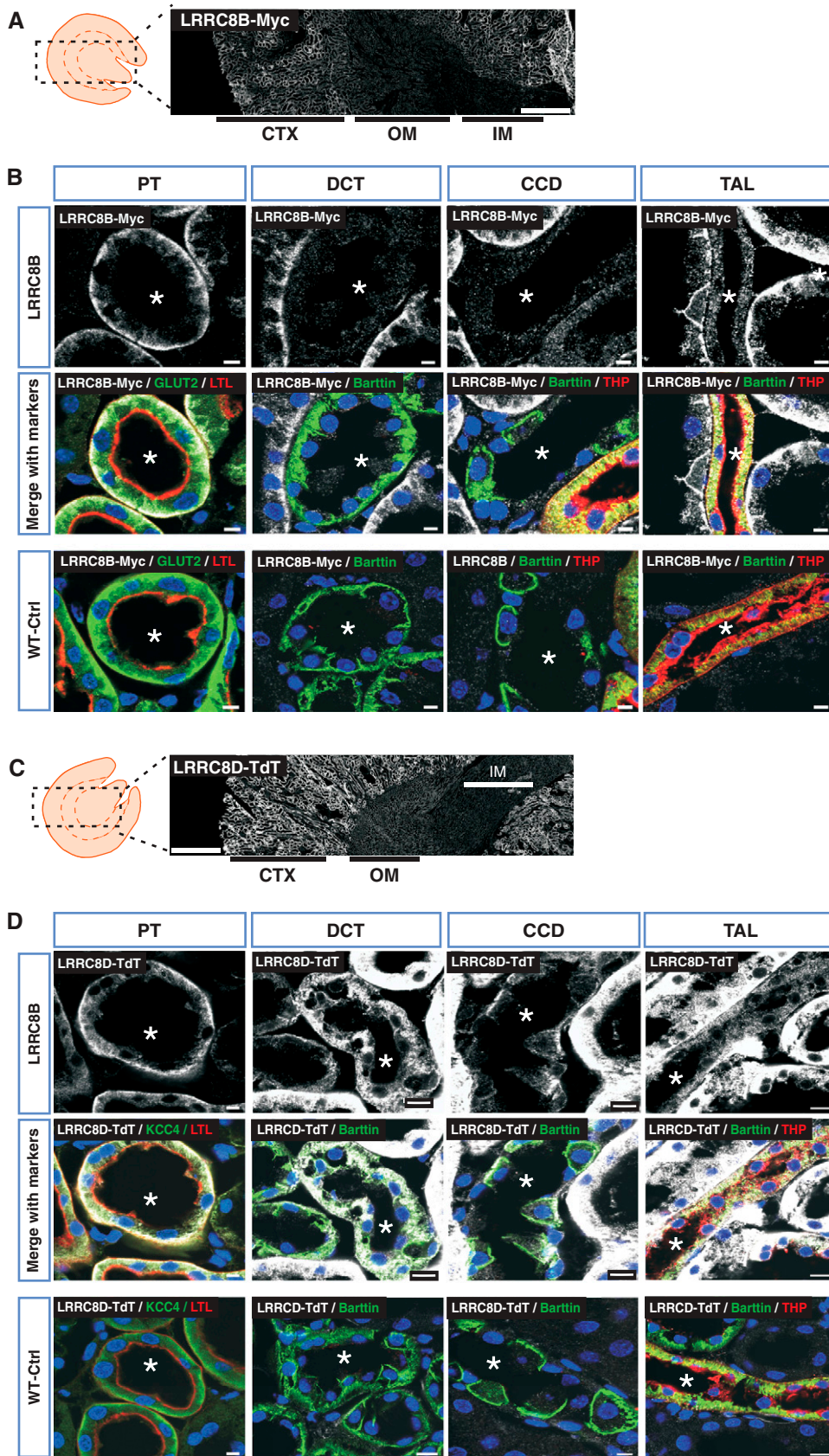


**Figure 2. Prominent expression of LRR8B and LRR8D in basolateral membranes of PTs.** (A) LRR8B-smFPMyc detection (white) in *Lrrc8b*<sup>smFPMyclox/smFPMyclox</sup> kidney, using a Myc antibody. (B) Immunodetection of LRR8B-smFPMyc (in white) in different

**Figure 2.** (Continued) renal tubules. LRRC8B-smFPMyc is prominently found at the basolateral membrane of the PT with weaker expression in the TAL, but was not detected in the DCT and CCD. (C) Overview of renal LRRC8D-TdTomato expression in *Lrrc8d<sup>fT<sup>Lox</sup>/T<sup>dLox</sup></sup>* mice, detected with an RFP antibody (white). (D) Localization of LRRC8D-TdTomato (white) in different nephron segments. In (A) and (C), kidney cortex (CTX), outer medulla (OM), and inner medulla (IM) are indicated. In (B) and (D), an asterisk indicates lumen of the tubule. PT was identified with *Lotus tetragonolobus* Lectin (LTL) at the brush border (red) and GLUT2 or KCC4 (green) at the basolateral membrane. DCT recognized by the basolateral staining of Barttin (green), which also expresses in ICs of CCD and TAL. TAL was additionally labeled with Tamm–Horsfall protein (THP, red) at the apical membrane. Myc and RFP-specific signal was tested in WT mice (WT-Ctrl). Nuclei stained with DAPI (blue). Scale bars, 10  $\mu$ m (DCT, TAL), 5  $\mu$ m (CCD, PT), and 500  $\mu$ m (whole kidney). Images are representative of  $n \geq 3$  mice per genotype.

was assessed using Mann–Whitney *U* test in Prism, Graph-Pad Software. A *P* value  $< 0.05$  was considered statistically significant.

## RESULTS

### Renal Expression Pattern of LRRC8 VRAC Subunits

Western blots indicated that all five LRRC8 VRAC subunits are expressed in the kidney (Figure 1A, Supplemental Figure 1A). The essential LRRC8A subunit appeared uniformly distributed between cortex, medulla, and papilla. LRRC8B and LRRC8D expression were moderately skewed toward the cortex, whereas LRRC8C and LRRC8E were predominantly found in inner medulla/papilla.

Because our LRRC8 antibodies do not work in formaldehyde-fixed tissue, we resorted to knockin mice expressing LRRC8 subunits fused to epitope tags at their carboxy termini. Electrophysiologic analysis of heterologously expressed channels showed that epitope addition did not change biophysical channel properties<sup>30</sup> (data not shown).

For LRRC8A, we used *Lrrc8a<sup>HAlox/HAlox</sup>* mice.<sup>30</sup> The modified allele was floxed to allow cell-type-specific deletion. The epitope tag produced no significant alteration in the intrarenal distribution of LRRC8A (Supplemental Figure 1B). Consistent with Western blots (Figure 1A), staining for the HA epitope appeared overall homogeneous in kidney sections with a slight gradient from cortex to papilla (Figure 1B). LRRC8A-HA was found in renal tubules (Figure 1C), glomeruli (Figure 1D), and vasculature (Supplemental Figure 2). Labeling specificity was ascertained using wild-type (WT) mice as negative control (Figure 1, C and D).

Deleting LRRC8A-HA specifically in endothelium with Tie2-Cre mice<sup>36</sup> revealed that the medullary LRRC8A-HA signal largely stems from vasculature (Supplemental Figure 2). PTs showed highest LRRC8A expression. LRRC8A resided in basolateral membranes (Figure 1C). Minor amounts of LRRC8A-HA were detected in thick ascending limb (TAL), in distal convoluted tubule (DCT), and in apparently all cell types of the cortical collecting duct (CCD) (Figure 1C). It was difficult to unambiguously detect LRRC8A in the thin limb by immunohistochemical staining, but mRNA expression studies confirm its presence in this segment.<sup>41</sup> Contradictory reports described VRACs also on lysosomes,<sup>42,43</sup> but LRRC8A-HA

did not colocalize with LAMP1 in either PT cells or ICs. (Supplemental Figure 3).

Likewise, LRRC8B (tagged with smFPMyc<sup>31</sup>) was prominently expressed in basolateral membranes of PTs (Figure 2, A and B, Supplemental Figure 1C). At lower levels it was also found in TAL, but not in DCT or CCD. The expression pattern of LRRC8D closely resembled that of LRRC8A. The tdTomato-labeled LRRC8D subunit<sup>29</sup> was prominently expressed in basolateral membranes of PTs. It was also found to a minor degree in TAL, DCT, and CCD (Figure 2, C and D, Supplemental Figure 1D).

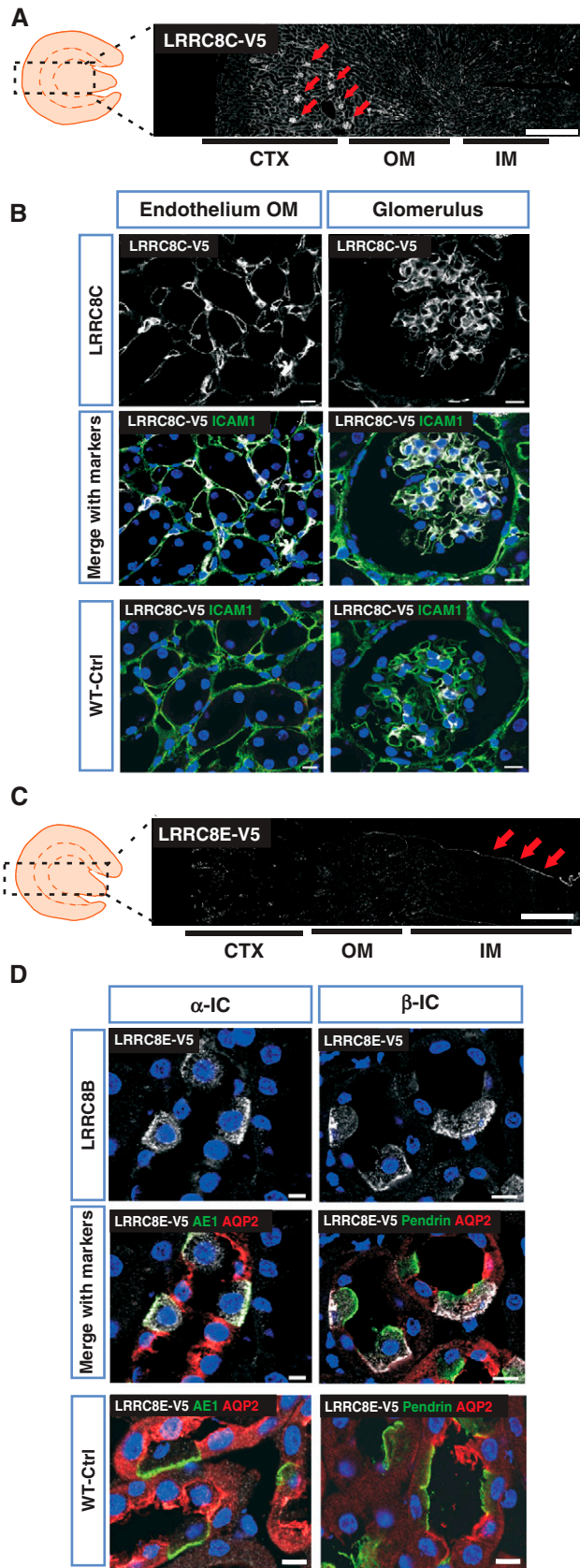
LRRC8C-V5 was not detected in renal tubules, but was prominently expressed in vascular endothelial cells (Figure 3, A and B). LRRC8E, tagged with smFPV5,<sup>31</sup> was mostly detected in the urothelial lining of the papilla (Figure 3C), explaining the expression pattern observed in Western blots (Figure 1A, Supplemental Figure 1E). LRRC8E was also present in scattered cells in cortex and medulla. These were identified as acid-secreting  $\alpha$ - and bicarbonate-secreting  $\beta$ -ICs by the expression of AE1 and pendrin, respectively (Figure 3D). LRRC8E was found in basolateral membranes in addition to fine cytoplasmic punctae. It could not be detected in Na<sup>+</sup>- and water-reabsorbing principal cells identified by AQP2.

Table 1 summarizes the expression patterns of LRRC8A–E subunits.

### Tubular Injury upon Disruption of *Lrrc8a*

Constitutive *Lrrc8a<sup>-/-</sup>* mice display high pre- and perinatal lethality and multiorgan pathology.<sup>44</sup> We therefore used *Lrrc8a<sup>lox/lox</sup>* or *Lrrc8a<sup>HAlox/HAlox</sup>* mice crossed with Cre recombinase-expressing mouse lines to delete LRRC8A, and hence total VRAC activity, in specific cell types. Crosses with ApoE-Cre mice, which delete target genes along the nephron in a chimeric fashion<sup>45–47</sup> (Figure 4A), reduced LRRC8A protein levels in both cortex and medulla by approximately 50% (Figure 4B), a finding confirmed by immunofluorescence (Figure 4, D and E). Deletion was chimeric in tubules, glomeruli, and blood vessels (Figure 4E).

ApoE-Cre;*Lrrc8a<sup>lox/lox</sup>* mice displayed scattered renal injury. It was most prominent in cortex and mainly affected PTs with swollen cells, dilatation, and sometimes collapse of tubules. In more distal nephron segments luminal casts and



**Figure 3. Renal expression pattern of LRRC8C and LRRC8E.**

(A) V5-tagged LRRC8C (white) in knockin *Lrrc8c*<sup>V5/V5</sup> mouse, using a V5 antibody. Glomerulus are indicated with arrows. (B) LRRC8C-V5 (in white) colocalized with the endothelial marker ICAM1 (green) in outer medulla (OM) and glomerulus. (C) Renal expression of LRRC8E-smFPV5 in *Lrrc8e*<sup>smFPV5/smFPV5</sup> knockin mice, using a V5 antibody. Prominent urothelium staining (arrows), and scattered staining in medulla and cortex which represent ICs as seen in (D). (D) LRRC8E-V5 (in white) is expressed in basolateral membranes of ICs, identified as  $\alpha$ -IC by AE1 (green) and  $\beta$ -IC by pendrin (green). LRRC8E-V5 was not found in principal cells (stained with AQP2 in red). In (A) and (B), cortex (CTX), outer medulla (OM), and inner medulla (IM) are indicated below. V5 signal specificity was tested in WT mice (WT-Ctrl), nuclei stained with DAPI (blue). Scale bars, 10  $\mu$ m (glomerulus, DCT, PT), 5  $\mu$ m (CCD, TAL), and 500  $\mu$ m (whole kidney). Images are representative of at least three mice per genotype.

nearby damaged cells were observed (Figure 4F). Electron microscopy revealed several dedifferentiation states in single PT sections, including brush border loss, cell swelling, substantial thickening of basement membranes, organelle rarefaction, mitochondrial damage, and hydropic cell death (Supplemental Figure 4, A and B). Interstitial fibrosis was detected by trichrome staining (Figure 4F). However, we also found apparently healthy PT cells that lacked LRRC8A (Figure 4E). Hence some cells, for unknown reasons, were resistant to VRAC disruption, or, more likely, cellular proliferation continuously replaced slowly degenerating cells.<sup>48</sup> Indeed, the proliferation marker Ki67<sup>49</sup> was markedly upregulated in cortex of ApoE-Cre;*Lrrc8a*<sup>HAllox/HAllox</sup> kidneys (Supplemental Figure 5).

*Pax8*-rtTACre mice were used to acutely induce *Lrrc8a* deletion in epithelial cells along the entire nephron<sup>37</sup> (Supplemental Figure 6A). Doxycycline treatment of adult *Pax8*-rtTACre;*Lrrc8a*<sup>lox/lox</sup> mice reduced LRRC8A levels by approximately 70% and approximately 30% in cortex and medulla, respectively (Supplemental Figure 6B). Immunohistochemistry confirmed high deletion efficiency along the nephron while sparing glomeruli and vasculature (Supplemental Figure 6, D and E). Kidney injury was similar to that of ApoE-Cre;*Lrrc8a*<sup>HAllox/HAllox</sup> mice (Supplemental Figure 6F). Hence, the observed kidney injury does not require *Lrrc8a* disruption during development.

### Renal Pathophysiology in Mice Lacking LRRC8A

Adult ApoE-Cre;*Lrrc8a*<sup>lox/lox</sup> mice, but not acutely induced *Pax8*-rtTACre;*Lrrc8a*<sup>lox/lox</sup> mice, weighed slightly less than control littermates (Figure 4C, Supplemental Figure 6C). Both mouse models had reduced GFR and increased serum creatinine (Supplemental Table 2), although only ApoE-Cre, but not *Pax8*-rtTACre, drives disruption in glomeruli.

**Table 1.** Different expression patterns of VRAC subunits in the nephron

VRAC Subunit	Glomerulus	Proximal Tubule	Thick Ascending Limb	Distal Tubule	Cortical Collecting Duct
LRR8A	+++	+++	+	+	+ (ICs and PCs)
LRR8B	++	+++	+	–	–
LRR8C	+++	–	–	–	–
LRR8D	–	+++	+	+	+ (ICs and PCs)
LRR8E	–	–	–	–	+++ (ICs)

Qualitative estimation of abundance from highest (+++) to absence (–). IC, intercalated cell; PC, principal cell.

This suggests that these changes may result from tubuloglomerular feedback rather than from alterations in glomeruli (Supplemental Figure 4C).

Both mouse lines displayed mild proteinuria (Supplemental Figure 7A) which was less pronounced than in control *Clcn5*<sup>+/–</sup> mice with a specific impairment of PT endocytosis.<sup>47</sup> Both lines also showed mild glycosuria (Supplemental Table 3) despite normal expression levels of major glucose transporters (Supplemental Figure 8). Increases in urinary phosphate and ammonia were not significant and urinary uric acid was normal (Supplemental Table 3). By contrast, urine pH was significantly lower in ApoE-Cre;*Lrrc8a*<sup>lox/lox</sup> mice.

Unexpectedly, both mouse lines had markedly increased diuresis and water intake under free access to water (Figure 4, G and H and Supplemental Figure 6, G and H for ApoE-Cre;*Lrrc8a*<sup>lox/lox</sup> and induced Pax8-rtTACre;*Lrrc8a*<sup>lox/lox</sup>, respectively). Urine osmolality was approximately halved with both lines. Total urinary excretion of Na<sup>+</sup>, K<sup>+</sup>, and Cl<sup>–</sup> appeared marginally increased, but this difference did not reach statistical significance in most cases (Supplemental Table 3). Renal expression levels of relevant ion transport proteins were unchanged in ApoE-Cre;*Lrrc8a*<sup>lox/lox</sup> mice (Supplemental Figures 8 and 9). Under 24-hour water restriction, both conditional *Lrrc8a* KO lines could concentrate urine, but less than control littermates (Figure 4H, Supplemental Figure 6H), and had increased blood Na<sup>+</sup> and Cl<sup>–</sup> concentrations as sign of dehydration (Supplemental Table 4).

Secretion of antidiuretic vasopressin (AVP) in the supra-optical nucleus may be modulated by VRAC-mediated taurine release from astrocytes.<sup>4,50</sup> Because the ApoE promoter is active in some glial cells,<sup>51</sup> we wanted to exclude central effects of *Lrrc8a* disruption. Serum concentrations of copeptin, a surrogate of AVP,<sup>52</sup> were indistinguishable between WT and ApoE-Cre;*Lrrc8a*<sup>lox/lox</sup> mice with free access to water (68.3±16 pg/ml and 69.7±13 pg/ml, respectively), and rose about 7-fold upon 24-hour water restriction in either genotype (442±36 [control] and 539±60 pg/ml [ApoE-Cre;*Lrrc8a*<sup>lox/lox</sup>]). Differences in protein levels of AQP2 and pAQP2(S269), which is inserted into apical membranes of principal cells in response to AVP,<sup>53</sup> did not reach statistical significance between genotypes (Supplemental Figure 10). Water reabsorption through AQP2 is driven by the hyperosmolarity of the medulla.<sup>54</sup> Osmolarity

of dissected medulla from euhydrated ApoE-Cre;*Lrrc8a*<sup>lox/lox</sup> mice was decreased by approximately 20% compared with controls (Supplemental Figure 11A). Upon water deprivation, the osmolarity increased about 2- to 3-fold in either genotype (Supplemental Figure 11A), but remained approximately 30% lower in the KO mainly due to lower Na<sup>+</sup> concentrations (Supplemental Figure 11, B–E). Collectively, these data indicate that increased diuresis of ApoE-Cre;*Lrrc8a*<sup>lox/lox</sup> mice is not secondary to changes in central osmoregulation, but can be, in part, attributed to decreased osmolarity of the medulla.

#### Distal Tubular Deletion of *Lrrc8a* Has Minimal Effects on Diuresis and Water Intake

To address a potential role of distal tubular VRACs, we deleted *Lrrc8a* in TAL and CD using Ksp-Cre mice<sup>55</sup> (Figure 5A). This reduced overall medullary LRR8A by only approximately 25% (Figure 5B), consistent with high LRR8A expression in medullary capillaries (Supplemental Figure 2). Immunostaining of medulla confirmed efficient LRR8-HA deletion in the nephron and unchanged expression in vasculature (Figure 5E). Renal morphology appeared normal (Figure 5F). Water intake, diuresis, and urine osmolality, both with water *ad libitum* or upon water restriction, did not differ between Ksp-Cre;*Lrrc8a*<sup>lox/lox</sup> mice and control littermates (Figure 5, G and H).

#### Villin-Cre Crosses Partially Recapitulate ApoE-Cre- or Pax8-rtTACre-Generated Phenotypes

Because the above results pointed to a proximal origin of VRAC-related renal pathology, we disrupted *Lrrc8a* using Villin-Cre mice<sup>33,56</sup> which in kidney exclusively deletes in PT<sup>57</sup> (Figure 6A). *Lrrc8a* disruption in PTs occurred with approximately 50% mosaicity (Figure 6, B, D, and E), resulting in overall 25% decrease of LRR8A levels in cortex and no change in medulla (Figure 6B). Villin-Cre;*Lrrc8a*<sup>HAllox/HAllox</sup> kidneys displayed less structural damage than mice with ApoE-Cre- or Pax8-rtTACre-driven *Lrrc8a* disruption. No protein casts were found in distal segments. Injury was restricted to renal cortex. PTs displayed some swollen cells, but renal cortex lacked fibrosis and glomeruli appeared normal (Figure 6F). The weight of Villin-Cre;*Lrrc8a*<sup>HAllox/HAllox</sup> mice appeared unchanged (Figure 6C). Similar to ApoE-Cre and Pax8-rtTACre models, Villin-Cre;*Lrrc8a*<sup>HAllox/HAllox</sup> mice exhibited increased diuresis, with urine osmolality being

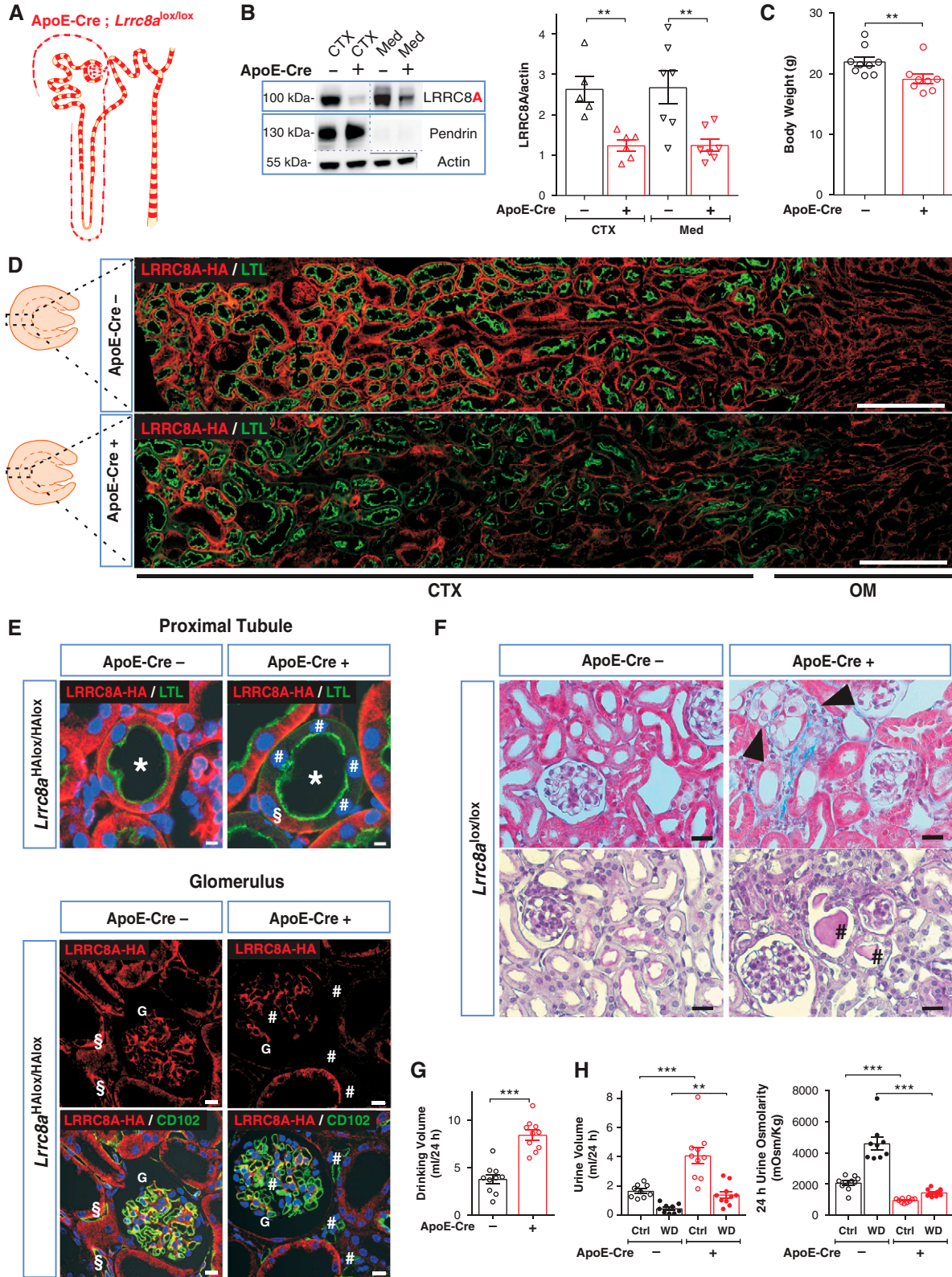


**Figure 4.** Disruption of the essential VRAC subunit LRRC8A results in hypoosmolar polyuria in ApoE-Cre;*Lrrc8a*<sup>lox/lox</sup> mice. (A) Sketch of chimeric *Lrrc8a* disruption both in nephron and blood vessels driven by ApoE-Cre. (B) Left, Western blot analysis of LRRC8A expression in kidney cortex (CTX) and medulla (Med) from ApoE-Cre;*Lrrc8a*<sup>lox/lox</sup> and control (*Lrrc8a*<sup>lox/lox</sup>) mice. Pendrin served as marker for cortex and  $\beta$ -actin as loading control. Right, Western blot quantification. (C) Body weight of control and

**Figure 4.** (Continued) ApoE-Cre 11- to 12-week-old siblings. (D) Assessment of ApoE-Cre-driven LRRC8A deletion by immunofluorescence (IF), using HA labeling (red) of kidney sections from ApoE-Cre;*Lrrc8a*<sup>HAlox/HAlox</sup> mice. *Lotus tetragonolobus* Lectin (LTL), marker (green) for apical membranes of PTs. Cortex (CTX) and outer medulla (OM) indicated below images. Scale bar, 200  $\mu$ m. (E) Upper panel, chimeric deletion of LRRC8A-HA in ApoE-Cre;*Lrrc8a*<sup>HAlox/HAlox</sup> mice detected by IF; absence of basolateral LRRC8A-HA (red) in some (#) and presence in other (§) cells of the same PT (\*) identified by LTL (green). Lower panel, chimeric deletion of LRRC8A in glomerulus (G) and endothelial cells labeled with CD102 (green); absence of LRRC8A-HA shown by # and LRRC8A-HA expression in endothelial cells of control by §. Nuclei are DAPI stained (blue). Scale bar, 5  $\mu$ m. (F) Upper panel, Masson's trichrome staining of cortex from control and ApoE-Cre mice. ApoE-Cre mice displayed tubular injury with mild fibrosis (blue), and swollen cells (black arrowheads). Lower panel, periodic acid-Schiff staining indicated hyaline casts (#). Scale bar, 20  $\mu$ m. (G) Daily water intake of ApoE-Cre and control mice. (H) Volume and osmolarity of 24-hour urine of ApoE-Cre and control mice with water *ad libitum* (Ctrl) or under 24-hour water restriction (WD). Bars, mean  $\pm$  SEM, \*\* $P < 0.01$ , \*\*\* $P < 0.001$  (Mann-Whitney *U* test). Images are representative of at least three mice per genotype.

approximately halved (Figure 6, G and H). Likewise, these mice concentrated urine upon water restriction, albeit less efficiently than controls. Comparison of ApoE-Cre and Pax8-rtTACre with Villin-Cre mouse models suggests a correlation between the severity of PT injury and functional deficits. This applied also for glycosuria (Supplemental Table 3) and proteinuria, which were quite variable between mice (Supplemental Figure 7B).

#### Similar Kidney Injury and Impaired Water Handling in *Lrrc8d*<sup>-/-</sup> Mice

Unlike *Lrrc8a*<sup>-/-</sup> mice, animals lacking any of the other four subunits survive well. Constitutive *Lrrc8e*<sup>-/-</sup> mice<sup>27</sup> and newly generated *Lrrc8b*<sup>-/-</sup> and *Lrrc8c*<sup>-/-</sup> mice had normal renal morphology (data not shown) and lacked other obvious phenotypes (Supplemental Tables 5 and 6). In contrast, *Lrrc8d*<sup>-/-</sup> mice (Figure 7A), whose weight did not differ from controls (Figure 7B), showed renal injury (Figure 7E) qualitatively similar to, but milder than, that found with ApoE-Cre- or Pax8-rtTACre-driven *Lrrc8a* disruption. Serum creatinine (0.11  $\pm$  0.003 mg/dl [WT] and 0.11  $\pm$  0.005 mg/dl [KO]) and GFR (274  $\pm$  16  $\mu$ l/min [WT] and 246  $\pm$  20  $\mu$ l/min [KO]) were unchanged between genotypes. *Lrrc8d*<sup>-/-</sup> mice recapitulated the hypoosmolar polyuria and increased water intake (Figure 7, C and D) and glycosuria (Supplemental Table 7). Increased blood Na<sup>+</sup> and Cl<sup>-</sup> concentrations as sign of dehydration were observed after 24-hour water deprivation (Supplemental Table 8).

#### Renal Tubular Injury Occurs within a Few Days after *Lrrc8a* Disruption

Already four days after initiating doxycycline treatment of Pax8-rtTACre;*Lrrc8a*<sup>lox/lox</sup> mice, LRRC8A declined by approximately 50% and some PT cells were damaged. LRRC8A abundance declined further with prolonged treatment and was accompanied by progressive tissue injury. Tissue damage proceeded after stopping doxycycline administration, as expected from slowly developing cellular degeneration after VRAC disruption. The development of

polyuria roughly correlated with the extent of kidney injury (Supplemental Figure 12), suggesting that a potential impairment of transepithelial transport in *Lrrc8a*-disrupted, but morphologically still intact, epithelial cells contributes little to these phenotypes.

#### Organic VRAC Substrates Accumulate in Kidney Cortex upon Loss of LRRC8A

To examine whether loss of VRACs leads to cytosolic accumulation of metabolites that no longer can leave PT cells, we surveyed metabolites in kidney cortex of ApoE-Cre;*Lrrc8a*<sup>lox/lox</sup> mice and control siblings. In addition to other changes, several known VRAC substrates<sup>3,5,19,20,25,58,59</sup> such as taurine, *myo*-inositol, gluconate, and lactate were significantly increased in LRRC8A-depleted cortex (Supplemental Figure 13). However, almost no significant changes in metabolite concentrations were found in *Lrrc8d*<sup>-/-</sup> cortex. This observation correlates with the less severe cortical damage of *Lrrc8d*<sup>-/-</sup> mice and agrees with the fact that only LRRC8A, but not LRRC8D, is essential for VRAC activity.<sup>20</sup>

## DISCUSSION

Large alterations in osmolarity occurring during changes in diuresis require efficient renal cell volume regulation. A major player in this process are VRACs, which transport chloride and organic osmolytes.<sup>4,19</sup> We now mapped the renal expression pattern of all five LRRC8 subunits of heteromeric VRACs<sup>20</sup> and explored their renal function in genetic mouse models. Except for LRRC8C, which was restricted to vascular endothelium, all subunits were found in tubular epithelial cells, albeit with strikingly distinct expression patterns. Unexpectedly, VRACs were most highly expressed in the proximal rather than distal nephron despite renal medulla experiencing the largest changes in osmolarity. Degeneration of PT cells lacking VRACs was associated with increased diuresis and symptoms of proximal tubular dysfunction. VRACs are essential for the homeostasis of the highly transporting PT.

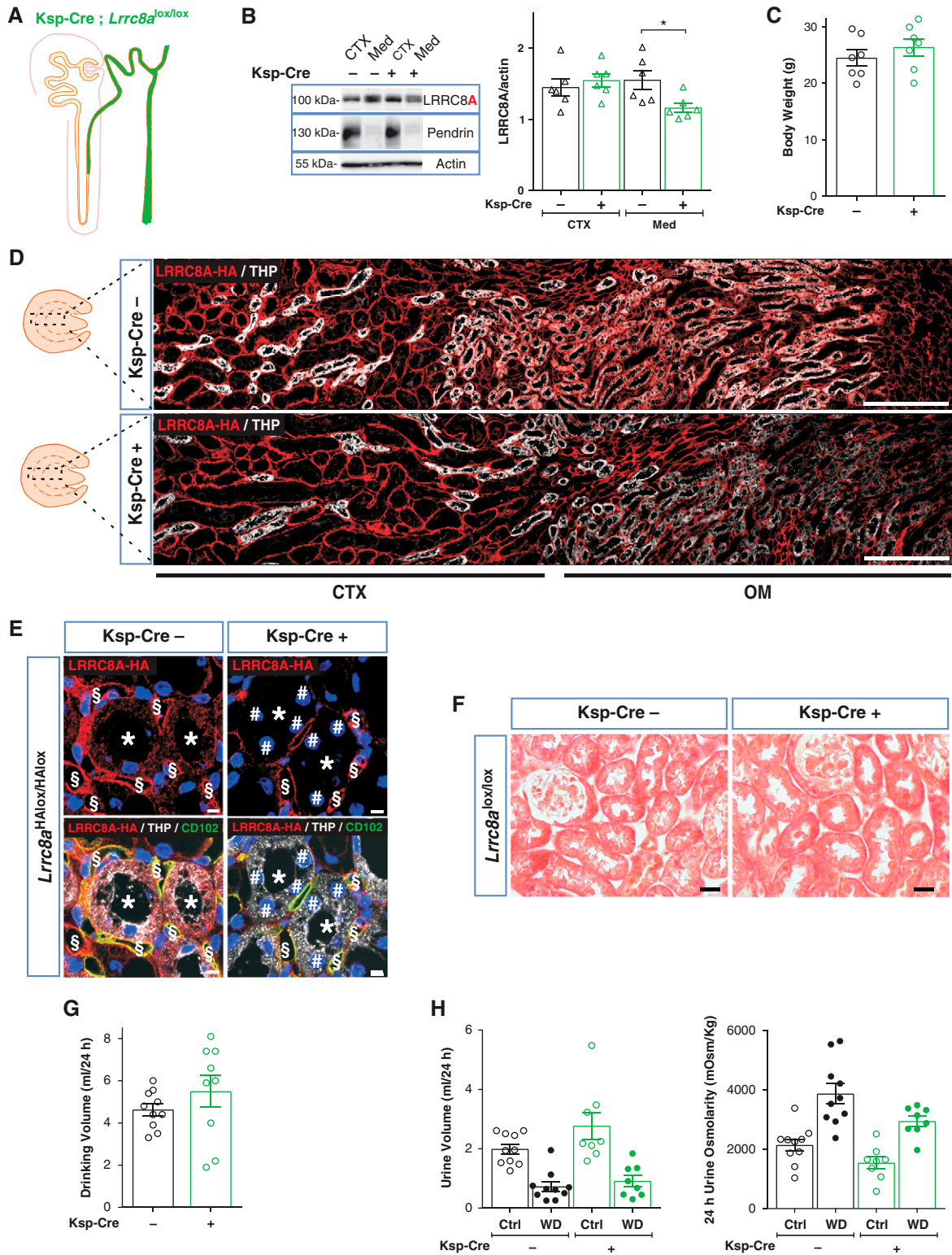


**Figure 5. Distal deletion of LRRC8A by Ksp-Cre does not affect urine concentration ability.** (A) Sketch of Ksp promoter-driven Cre expression. (B) Left, Western blot analysis of LRRC8A expression in cortex (CTX) and medulla (Med) in Ksp-Cre;*Lrrc8a<sup>lox/lox</sup>* and control (*Lrrc8a<sup>lox/lox</sup>*) mice. Pendrin, cortex marker;  $\beta$ -actin, loading control. Right, Western blot quantification. (C) Body weight of control and Ksp-Cre 11- to 12-week-old siblings. (D) Assessment of Ksp-Cre-driven LRRC8A deletion by HA labeling (red) of kidney sections from Ksp-Cre;*Lrrc8a<sup>HAlox/HAlox</sup>* mice. TALs labeled (in white) for apical Tamm–Horsfall protein (THP). Approximate extension

**Figure 5.** (Continued) of cortex and outer medulla indicated below. Scale bar, 200  $\mu\text{m}$ . (E) Efficient deletion (#) of HA-tagged LRRC8A (red) in TAL (\*; labeled in white with THP in lower panels) in Ksp-Cre;*Lrrc8a*<sup>lox/lox</sup> mice. Note the faint red LRRC8A-HA staining in control, which is absent from Ksp-Cre tubules. Ksp-Cre did not delete in blood vessels (detected with endothelial CD102 [in green, §]). Nuclei are DAPI stained (blue). Scale bar, 5  $\mu\text{m}$ . (F) Masson's trichrome staining of kidney cortex fails to detect fibrosis. Scale bar, 20  $\mu\text{m}$ . (G) Daily water intake of Ksp-Cre;*Lrrc8a*<sup>lox/lox</sup> and control mice. (H) Volume and osmolality of 24-hour urine of Ksp-Cre and control mice with water *ad libitum* (Ctrl) or under 24-hour water restriction (WD). Bars, mean  $\pm$  SEM, \* $P < 0.05$  (Mann-Whitney U test). Pictures are representative of at least three mice per genotype.

### Expression Pattern of LRRC8 Subunits

Agreeing with the near-ubiquitous presence of VRAC currents,<sup>5,19</sup> LRRC8A is apparently expressed in every renal cell type, although at markedly different levels. LRRC8A expression was highest in PTs and vascular endothelium. The latter cells specifically express LRRC8C. LRRC8A/C channels transport many substrates,<sup>25,27,28,58</sup> but no morphologic alterations were found in *Lrrc8c*<sup>-/-</sup> or endothelium-specific *Lrrc8a*<sup>-/-</sup> mice. This argues against a suggested crucial role of vascular endothelial VRACs in angiogenesis.<sup>60</sup>

LRRC8E showed remarkably specific expression in the urothelium and ICs. Besides being efficient  $\text{Cl}^-$  channels, LRRC8A/E heteromers transport organic substrates with a preference for negatively charged ones such as aspartate and glutamate,<sup>25,58,59</sup> ATP,<sup>58</sup> and cGAMP,<sup>27,28</sup> but it is unclear whether ICs need this particular transport function. ICs appeared structurally normal in both Ksp-Cre;*Lrrc8a*<sup>lox/lox</sup> and *Lrrc8e*<sup>-/-</sup> mice (data not shown) and urinary pH was normal in both lines suggesting that their transport of acid was not affected.

LRRC8A, LRRC8B, and LRRC8D showed highest expression in PTs where they colocalized in basolateral membranes. Immunofluorescence is ill suited to determine their relative expression levels, but semiquantitative RNA sequencing data<sup>41</sup> suggest that LRRC8D is prevalent in PTs (LRRC8A:LRRC8B:LRRC8D approximately 1:3:20). Because LRRC8A is required for the plasma membrane expression of all other subunits,<sup>20</sup> this expression ratio indicates a predominant presence of LRRC8A/D and LRRC8A/B/D channels. LRRC8D ablation will leave poorly transporting LRRC8A/B channels<sup>20,58</sup> in PTs.

Although largely agreeing with mRNA expression levels in microdissected mouse nephron segments,<sup>41</sup> our study examined expression at the protein level and provides important information on the subcellular localization and presence in specific cell types.

### Origin of Proximal Tubular Degeneration

LRRC8-related cell damage was most evident in PTs. Crosses with Villin-Cre mice suggested that it may be a cell-intrinsic consequence of *Lrrc8a* gene ablation. When *Lrrc8a* disruption included the distal nephron, as with ApoE- or Pax8-driven disruption, we observed additional distal injury associated with Tamm-Horsfall protein-positive luminal protein casts. These may be secondary to

solute overload caused by impaired PT reabsorption, which is more severe with ApoE- or Pax8- than with Villin-driven disruption. Although Ksp-Cre;*Lrrc8a*<sup>lox/lox</sup> mice showed that distal *Lrrc8a* disruption is insufficient to cause pathology, we cannot exclude that it contributes to distal tubular injury together with PT disruption.

PTs absorb about 70% of filtered salt and water. Although not exposed to large changes in extracellular osmolality, an imbalance between apical uptake and basolateral transport may cause cell swelling that might need VRACs for RVD. Indeed, some *Lrrc8a*<sup>-/-</sup> PT cells appeared swollen (Figures 4F and 6F, Supplemental Figure 6F), reminiscent of swollen and finally dying spermatids in germ cell-specific *Lrrc8a* KO mice.<sup>30</sup> Hence impaired cell volume regulation might contribute to PT injury.

However, compared with PTs, medullary cells experience much larger osmotic stress.<sup>1,2,61</sup> When exposed to hyperosmolality, they accumulate osmolytes such as betaine, taurine, and *myo*-inositol.<sup>9</sup> These compounds are substrates of VRACs<sup>19,25,26</sup> through which they may leave cells when osmolality drops again. In contrast to PTs, medullary cells were not damaged upon VRAC ablation. By extrapolation, impaired RVD may not be the major factor leading to PT injury, a notion bolstered by the fact that loss of KCC3 and KCC4, which are important for PT RVD, does not affect PT integrity.<sup>62</sup>

VRACs, which are partially open under isotonic conditions,<sup>26,27</sup> might also play a role in transepithelial transport. The PT reabsorbs  $\text{Cl}^-$  predominantly paracellularly, but there may also be a small component of transcellular  $\text{Cl}^-$  transport involving unidentified basolateral  $\text{Cl}^-$  channels<sup>63,64</sup> which might be embodied by VRACs. VRACs also conduct bicarbonate,<sup>58,65</sup> but a major role in transepithelial bicarbonate transport is implausible considering the prominent role of basolateral  $\text{NaHCO}_3$  symport in PT acid secretion.<sup>66,67</sup> A role of VRACs in apical  $\text{H}^+$ -secretion also seems unlikely because of the acidic urinary pH in the KO, although disruption of the basolateral NBCe1  $\text{NaHCO}_3$  cotransporter counterintuitively increases urinary acidification.<sup>68</sup> Also degeneration of PT cells should rather lead to more alkaline urine. Because we excluded a role of ICs, we have no explanation for the acidic urinary pH in *Lrrc8* KO mice.

We favor the hypothesis that impaired transport of organic compounds underlies PT pathology. LRRC8A and -D containing channels transport a plethora of organic

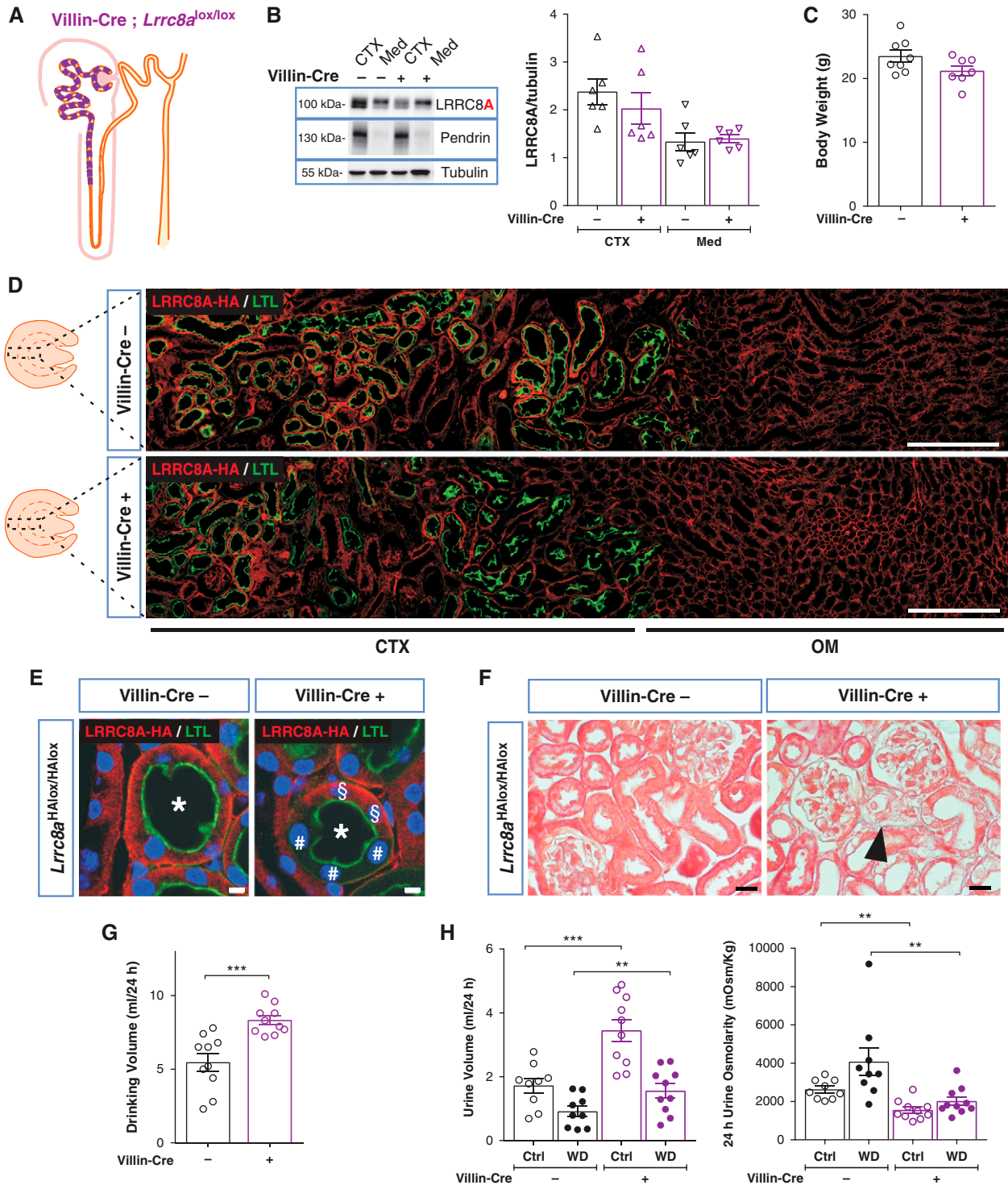


**Figure 6. Proximal tubular-restricted disruption of LRRC8A in Villin-Cre;*Lrrc8a*<sup>HAlox/HAlox</sup> mice results in polyuria and polydipsia.** (A) Sketch of chimeric deletion by Villin-Cre in the proximal nephron. (B) Left, Western blot analysis of LRRC8A expression in cortex (CTX) and medulla (Med) in Villin-Cre;*Lrrc8a*<sup>HAlox/HAlox</sup> and control (*Lrrc8a*<sup>HAlox/HAlox</sup>) mice. Pendrin, CTX marker; Tubulin, loading control. Right, Western blot quantification. (C) Body weight of control and Villin-Cre;*Lrrc8a*<sup>HAlox/HAlox</sup> 11- to 12-week-old siblings. (D) Assessment of Villin-Cre-driven LRRC8A deletion by HA labeling (red) of kidney sections from Villin-Cre;*Lrrc8a*<sup>HAlox/HAlox</sup> and control mice. PTs identified by *Lotus tetragonolobus* Lectin (LTL) (green). Quantification of deletion efficiency by cell counting yielded 48.7±2.6% in Villin-Cre;*Lrrc8a*<sup>HAlox/HAlox</sup> PT cells (using three images from two different mice). Cortex (CTX) and outer medulla (OM) indicated below. Scale bar, 200 μm. (E) Chimeric deletion (#) of basolateral HA-tagged LRRC8A (red) in Villin-Cre;*Lrrc8a*<sup>HAlox/HAlox</sup> mice. Cells expressing LRRC8A-HA indicated with §, nuclei stained with DAPI (blue). Scale bar, 5 μm. (F) Masson's trichrome staining

**Figure 6.** (Continued) of kidney cortex from control and Villin-Cre mice. Tubular injury in Villin-Cre mice with very mild fibrosis (blue), and few swollen cells (black arrowhead). Scale bar, 20  $\mu\text{m}$ . (G) Daily water intake in Villin-Cre;*Lrrc8a*<sup>lox/lox</sup> and control mice. (H) Volume and osmolarity of 24-hour urine of Villin-Cre and control mice with water *ad libitum* (Ctrl) or under 24-hour water restriction (WD). Bars, mean  $\pm$  SEM, \* $P < 0.05$ , \*\* $P < 0.01$ , \*\*\* $P < 0.001$  (Mann–Whitney *U* test). Pictures are representative of more than three mice per group.

substrates, irrespective of their electrical charge,<sup>25</sup> while displaying relatively low  $\text{Cl}^-$  currents. VRACs may also transport small peptides such as glutathione (GSH),<sup>69</sup> but we did not observe changes in glutathione in ApoE-Cre;*Lrrc8a*<sup>lox/lox</sup> mice: total GSH ( $\mu\text{g/g}$  tissue) =  $2.6 \pm 0.3$  (controls) and  $2.8 \pm 0.1$  (ApoE-Cre;*Lrrc8a*<sup>lox/lox</sup>); and glutathione disulfide (nmol/g tissue) =  $53.8 \pm 11$  (controls) and  $45.3 \pm 7.3$  (ApoE-Cre;*Lrrc8a*<sup>lox/lox</sup>). Many of these compounds are actively reabsorbed by apical cotransporters, accumulate in the cytosol, and passively leave across the basolateral membrane. If VRACs mediate their basolateral exit, their cytosolic concentrations will increase, potentially causing osmotic swelling or toxic effects. Consistent with the role of VRACs in taurine transport,<sup>25,26</sup> taurine and several other VRAC substrates were increased in the cortex of ApoE-Cre;*Lrrc8a*<sup>lox/lox</sup> (Supplemental Figure 13). Other

compounds were decreased, probably as a consequence of changed cellular metabolism. The transport activity of LRRC8A/B channels, the main heteromers remaining after *Lrrc8d* disruption, seems sufficient to prevent significant changes in cortical metabolites and correlates with milder injury in *Lrrc8d*<sup>-/-</sup> than in *Lrrc8a*<sup>-/-</sup> kidneys. Our measurements underestimate these metabolite changes because of cellular heterogeneity of kidney cortex and mosaic *Lrrc8* disruption, and because damaged PT cells may no longer retain these compounds. Secondary changes in transmembrane fluxes may also come into play. For instance, the decrease in cortical 1,5-anhydro-D-glucitol likely results from glycosuria because luminal glucose competes with 1,5-anhydro-D-glucitol uptake into the PT.<sup>70</sup> No single metabolite emerged as a candidate for explaining the observed cellular pathology. We therefore propose that

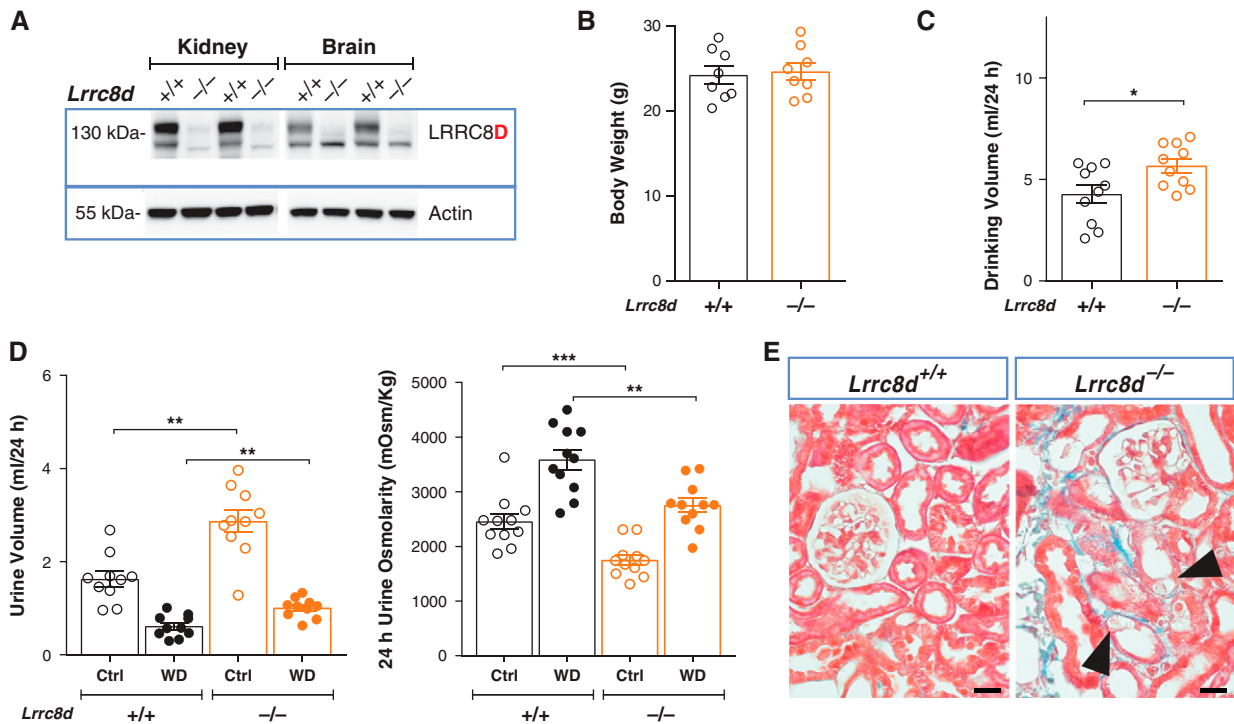


**Figure 7. Constitutive deletion of LRRC8D recapitulates the renal phenotype of proximal tubular deletion of LRRC8A.** (A) Representative Western blot analysis of LRRC8D expression in kidney and brain membrane fractions isolated from LRRC8D KO (*Lrrc8d*<sup>-/-</sup>) and WT mice;  $\beta$ -actin, loading control. (B) Body weight of 11- to 12-week-old *Lrrc8d*<sup>-/-</sup> and WT siblings. (C) Daily water intake of *Lrrc8d*<sup>-/-</sup> and WT mice. (D) Volume (left) and osmolarity (right) of 24-hour urine collected from *Lrrc8d*<sup>-/-</sup> and control mice, obtained with water *ad libitum* (Ctrl) or under 24-hour water restriction (WD). (E) Masson's trichrome staining of kidney cortex from *Lrrc8d*<sup>-/-</sup> and WT mice. Mild fibrosis in *Lrrc8d*<sup>-/-</sup> mice (blue), tubular injury and swollen cells are indicated (arrowheads). Scale bar, 20  $\mu\text{m}$ . Representative pictures of three mice per genotype. Bars, mean  $\pm$  SEM, \*\* $P < 0.01$ , \*\*\* $P < 0.001$  (Mann–Whitney *U* test).

accumulation of several substrates of VRACs jointly exert toxic effects and lead to kidney injury.

### Impact of VRAC Deletion on Kidney Function

PT disruption of *Lrrc8a* or *Lrrc8d* resulted in mild glycosuria, low molecular weight proteinuria, polyuria, and borderline hyperchloremic acidosis. No changes in the abundance of relevant transport proteins were observed. Impaired kidney function might rather result from the loss of viable PT cells as suggested by the parallel development of morphologic and functional changes upon acute *Lrrc8a* disruption. Functional effects conform largely to a set of variable symptoms of global PT dysfunction known as “Fanconi syndrome.”<sup>71,72</sup> For instance, the proteinuria of mice lacking *Lrrc8a* or *Lrrc8d* in the PT showed the typical pattern of proteins which are normally reabsorbed in the PT (transferrin, retinol- and VitD-binding proteins; Supplemental Figure 7). Urinary albumin, which like the aforementioned proteins is reabsorbed after binding to the megalin/cubilin complex,<sup>73</sup> was also increased. However, albuminuria was much less than expected for glomerular damage. Indeed, electron microscopy showed that the glomerular filter was largely intact even when *Lrrc8a* was partially disrupted in glomeruli by ApoE-Cre (Supplemental Figure 4C).

The most salient functional abnormality, polyuria, is found only in some “Fanconi” patients. Purely osmotic, glycosuria-related diuresis is excluded by decreased urine osmolarity of *Lrrc8a*-deficient mice. Because PTs reabsorb approximately 70% of filtered fluid, a decrease of PT water permeability might cause polyuria. Indeed, disruption of AQP1, the major water channel in both apical and basolateral membranes of the PT, severely impaired urine concentration ability.<sup>74,75</sup> This was, however, attributed to reduced medullary osmolarity, possibly owing to an overload of the counter-current system.<sup>74,75</sup> However, AQP1 appeared normal in ApoE-Cre;*Lrrc8a*<sup>lox/lox</sup> mice (Supplemental Figure 10). There is one report that VRACs also transport water,<sup>76</sup> but it seems unlikely that water transport through VRACs would reach levels comparable to AQP1. The slight decrease in osmolarity in euhydrated ApoE-Cre;*Lrrc8a*<sup>lox/lox</sup> mice might result from PT dysfunction and distal overload as in *Aqp1*<sup>-/-</sup> mice. In contrast to these mice, however, mice with PT disruption of *Lrrc8a* were still able, although less efficiently, to concentrate urine upon water deprivation, suggesting that the change in medullary osmolarity is more pronounced in *Aqp1*<sup>-/-</sup> mice.

Surprisingly, LRRC8/VRAC channels are crucial for the function and integrity of PT cells, but not for distal nephron segments that experience much larger changes in osmolarity. PT cells are particularly sensitive to harmful stimuli such as hypoxia or toxic drugs because of the large need for metabolic energy to reabsorb approximately two thirds of the glomerular filtrate. PT cells not only have the highest transport rates of the nephron, but by far transport

the most diverse set of molecules. We suggest that LRRC8A/D channels, which are particularly efficient in transporting a plethora of organic compounds, serve as nonspecific exit “valves” to prevent cellular accumulation of reabsorbed compounds or their metabolites. Their accumulation eventually leads to PT injury in mice lacking VRACs. By extension, we predict that VRACs protect, at least to some degree, PTs against drugs and toxins that are reabsorbed from the tubular lumen.

### DISCLOSURES

All authors have nothing to disclose.

### FUNDING

This work was supported by the European Research Council Advanced Grant VOLSIGNAL (#740537), the Deutsche Forschungsgemeinschaft (SFB 1365, B02), and Fondation Louis-Jeantet (Prix Louis-Jeantet de Médecine #2000) to T. Jentsch.

### ACKNOWLEDGMENTS

The authors thank Deborah Knecht (née Elger) for preliminary data; Felizia Voss for the generation of *Lrrc8b*<sup>smFPMyc/smFPMyc</sup> and *Lrrc8c*<sup>V5/V5</sup> knockin mice; Carolin Backhaus, Anika Günther, and Janet Liebold for excellent technical support; Adrian Schreiber for sharing transdermal GFR monitors; and many colleagues for sharing antibodies (see Supplemental Table 1).

### AUTHOR CONTRIBUTIONS

T. Jentsch, K. López-Cayuqueo, and R. Planells-Cases conceptualized the study, were responsible for formal analysis and investigation, and wrote the original draft; T. Jentsch was responsible for funding acquisition and supervision; S. Kempa was responsible for formal analysis; T. Jentsch and S. Kempa were responsible for resources; S. Bachmann, A. Oliveras, and M. Pietzke were responsible for investigation; K. López-Cayuqueo, M. Pietzke, and R. Planells-Cases were responsible for validation; and S. Bachmann, T. Jentsch, S. Kempa, K. López-Cayuqueo, M. Pietzke, and R. Planells-Cases were responsible for methodology and reviewed and edited the manuscript.

### DATA SHARING STATEMENT

All data are included in the manuscript and/or supporting materials.

### SUPPLEMENTAL MATERIAL

This article contains the following supplemental material online at <http://jasn.asnjournals.org/lookup/suppl/doi:10.1681/ASN.2021111458/-/DCSupplemental>.

Supplemental Table 1. Additional antibodies used throughout the study.

Supplemental Table 2. Serum creatinine and GFR of control, ApoE-Cre, Pax8-rtTACre, Ksp-Cre and Villin-Cre animals bred to *Lrrc8a*<sup>lox/lox</sup> mice.

Supplemental Table 3. Urinary pH and excretion rates of control and ApoE-Cre, Pax8-rtTACre, Ksp-Cre and Villin-Cre animals bred to *Lrrc8a*<sup>lox/lox</sup> mice, access to water *ad libitum*.

Supplemental Table 4. Blood and serum biochemical parameters after 24-hour water deprivation of control, ApoE-Cre, Pax8-rtTACre, Ksp-Cre and Villin-Cre animals bred to *Lrrc8a*<sup>lox/lox</sup> mice.

Supplemental Table 5. Urine parameter in *Lrrc8b*, *Lrrc8c*, and *Lrrc8e* KO and control littermates, with access to water *ad libitum*.

Supplemental Table 6. Blood parameter in *Lrrc8b*, *Lrrc8c*, and *Lrrc8e* KO and control littermates, with access to water *ad libitum*.

Supplemental Table 7. Urinary pH and excretion rates of control and *Lrrc8d* KO mice, access to water *ad libitum*.

Supplemental Table 8. Blood parameters after 24-hour water deprivation of control and *Lrrc8d* KO mice.

Supplemental Figure 1. Renal characterization of the LRRC8 VRAC subunits by Western blot.

Supplemental Figure 2. LRRC8A expression in renal medulla largely localizes to endothelial cells.

Supplemental Figure 3. LRRC8A and LRRC8D do not colocalize with the lysosomal/late endosomal marker LAMP1.

Supplemental Figure 4. Proximal tubular injury in ApoE-Cre;*Lrrc8a*<sup>lox/lox</sup> mice.

Supplemental Figure 5. Increased expression of the proliferation marker Ki67 in ApoE-Cre;*Lrrc8a*<sup>HAllox/HAllox</sup> mice.

Supplemental Figure 6. Acute deletion of LRRC8A in Pax8-rtTACre;*Lrrc8a*<sup>lox/lox</sup> mice recapitulates the renal phenotype of ApoE-Cre;*Lrrc8a*<sup>lox/lox</sup> mice.

Supplemental Figure 7. Mild proteinuria in ApoE-Cre and Pax8-rtTACre;*Lrrc8a*<sup>lox/lox</sup> mice.

Supplemental Figure 8. Normal protein abundance of SGLT2, SGLT1, and GLUT2 in ApoE-Cre;*Lrrc8a*<sup>lox/lox</sup> mice.

Supplemental Figure 9. Protein abundance of Na<sup>+</sup>/Cl<sup>-</sup> transporters and channels in renal cortex and medulla of ApoE-Cre;*Lrrc8a*<sup>lox/lox</sup> mice.

Supplemental Figure 10. Normal expression of aquaporins 1 and 2 in ApoE-Cre;*Lrrc8a*<sup>lox/lox</sup> mice.

Supplemental Figure 11. Interstitial inner medulla osmolarity and osmolyte concentrations of ApoE-Cre;*Lrrc8a*<sup>lox/lox</sup> mice and control siblings in euhydrated and 24-hour water restricted conditions.

Supplemental Figure 12. Progression of kidney injury after acute *Lrrc8a* deletion.

Supplemental Figure 13. Metabolomics analysis of several metabolites in ApoE-Cre;*Lrrc8a*<sup>lox/lox</sup> kidney cortex.

## REFERENCES

- Atherton JC, Hai MA, Thomas S: The time course of changes in renal tissue composition during water diuresis in the rat. *J Physiol* 197: 429–443, 1968
- Beck FX, Neuhofer W: Cell volume regulation in the renal papilla. *Contrib Nephrol* 152: 181–197, 2006
- Pasantes-Morales H: Channels and volume changes in the life and death of the cell. *Mol Pharmacol* 90: 358–370, 2016
- Jentsch TJ: VRACs and other ion channels and transporters in the regulation of cell volume and beyond. *Nat Rev Mol Cell Biol* 17: 293–307, 2016
- Hoffmann EK, Lambert IH, Pedersen SF: Physiology of cell volume regulation in vertebrates. *Physiol Rev* 89: 193–277, 2009
- Koivusalo M, Kapus A, Grinstein S: Sensors, transducers, and effectors that regulate cell size and shape. *J Biol Chem* 284: 6595–6599, 2009
- Garcia-Perez A, Burg MB: Renal medullary organic osmolytes. *Physiol Rev* 71: 1081–1115, 1991
- Burg MB, Garcia-Perez A: How tonicity regulates gene expression. *J Am Soc Nephrol* 3: 121–127, 1992
- Burg MB, Ferraris JD, Dmitrieva NI: Cellular response to hyperosmotic stresses. *Physiol Rev* 87: 1441–1474, 2007
- Cowley BD Jr, Ferraris JD, Carper D, Burg MB: In vivo osmoregulation of aldose reductase mRNA, protein, and sorbitol in renal medulla. *Am J Physiol* 258: F154–F161, 1990
- Uchida S, Kwon HM, Yamauchi A, Preston AS, Marumo F, Handler JS: Molecular cloning of the cDNA for an MDCK cell Na<sup>(+)</sup>- and Cl<sup>(-)</sup>-dependent taurine transporter that is regulated by hypertonicity. *Proc Natl Acad Sci U S A* 89: 8230–8234, 1992
- Yamauchi A, Uchida S, Kwon HM, Preston AS, Robey RB, Garcia-Perez A, et al.: Cloning of a Na<sup>(+)</sup>- and Cl<sup>(-)</sup>-dependent betaine transporter that is regulated by hypertonicity. *J Biol Chem* 267: 649–652, 1992
- Kwon HM, Yamauchi A, Uchida S, Preston AS, Garcia-Perez A, Burg MB, et al.: Cloning of the cDNAs for a Na<sup>+</sup>/myo-inositol cotransporter, a hypertonicity stress protein. *J Biol Chem* 267: 6297–6301, 1992
- Boettger T, Hübner CA, Maier H, Rust MB, Beck FX, Jentsch TJ: Deafness and renal tubular acidosis in mice lacking the K-Cl co-transporter *Kcc4*. *Nature* 416: 874–878, 2002
- Barrière H, Belfodil R, Rubera I, Tauc M, Lesage F, Poujeol C, et al.: Role of TASK2 potassium channels regarding volume regulation in primary cultures of mouse proximal tubules. *J Gen Physiol* 122: 177–190, 2003
- Rubera I, Tauc M, Bidet M, Poujeol C, Cuiller B, Watrin A, et al.: Chloride currents in primary cultures of rabbit proximal and distal convoluted tubules. *Am J Physiol* 275: F651–F663, 1998
- Meyer K, Korbmayer C: Cell swelling activates ATP-dependent voltage-gated chloride channels in M-1 mouse cortical collecting duct cells. *J Gen Physiol* 108: 177–193, 1996
- Boese SH, Glanville M, Gray MA, Simmons NL: The swelling-activated anion conductance in the mouse renal inner medullary collecting duct cell line mIMCD-K2. *J Membr Biol* 177: 51–64, 2000
- Nilius B, Eggermont J, Voets T, Buyse G, Manolopoulos V, Droogmans G: Properties of volume-regulated anion channels in mammalian cells. *Prog Biophys Mol Biol* 68: 69–119, 1997
- Voss FK, Ullrich F, Münch J, Lazarow K, Lutter D, Mah N, et al.: Identification of LRRC8 heteromers as an essential component of the volume-regulated anion channel VRAC. *Science* 344: 634–638, 2014
- Qiu Z, Dubin AE, Mathur J, Tu B, Reddy K, Miraglia LJ, et al.: SWELL1, a plasma membrane protein, is an essential component of volume-regulated anion channel. *Cell* 157: 447–458, 2014
- Deneka D, Sawicka M, Lam AKM, Paulino C, Dutzler R: Structure of a volume-regulated anion channel of the LRRC8 family. *Nature* 558: 254–259, 2018
- Nakamura R, Numata T, Kasuya G, Yokoyama T, Nishizawa T, Kusakizako T, et al.: Cryo-EM structure of the volume-regulated anion channel LRRC8D isoform identifies features important for substrate permeation. *Commun Biol* 3: 240, 2020
- Syeda R, Qiu Z, Dubin AE, Murthy SE, Florendo MN, Mason DE, et al.: LRRC8 proteins form volume-regulated anion channels that sense ionic strength. *Cell* 164: 499–511, 2016
- Lutter D, Ullrich F, Lueck JC, Kempa S, Jentsch TJ: Selective transport of neurotransmitters and modulators by distinct volume-regulated LRRC8 anion channels. *J Cell Sci* 130: 1122–1133, 2017
- Planells-Cases R, Lutter D, Guyader C, Gerhards NM, Ullrich F, Elger DA, et al.: Subunit composition of VRAC channels determines substrate specificity and cellular resistance to Pt-based anti-cancer drugs. *EMBO J* 34: 2993–3008, 2015
- Zhou C, Chen X, Planells-Cases R, Chu J, Wang L, Cao L, et al.: Transfer of cGAMP into bystander cells via LRRC8 volume-regulated anion channels augments STING-mediated interferon responses and anti-viral immunity. *Immunity* 52: 767–781.e6, 2020
- Lahey LJ, Mardjuki RE, Wen X, Hess GT, Ritchie C, Carozza JA, et al.: LRRC8A:C/E heteromeric channels are ubiquitous transporters of cGAMP. *Mol Cell* 80: 578–591.e5, 2020
- Stuhlmann T, Planells-Cases R, Jentsch TJ: LRRC8/VRAC anion channels enhance  $\beta$ -cell glucose sensing and insulin secretion. *Nat Commun* 9: 1974, 2018

30. Lück JC, Puchkov D, Ullrich F, Jentsch TJ: LRRC8/VRAC anion channels are required for late stages of spermatid development in mice. *J Biol Chem* 293: 11796–11808, 2018
31. Viswanathan S, Williams ME, Bloss EB, Stasevich TJ, Speer CM, Nern A, et al.: High-performance probes for light and electron microscopy. *Nat Methods* 12: 568–576, 2015
32. Leheste JR, Rolinski B, Vorum H, Hilpert J, Nykjaer A, Jacobsen C, et al.: Megalin knockout mice as an animal model of low molecular weight proteinuria. *Am J Pathol* 155: 1361–1370, 1999
33. el Marjou F, Janssen KP, Chang BH, Li M, Hindie V, Chan L, et al.: Tissue-specific and inducible Cre-mediated recombination in the gut epithelium. *Genesis* 39: 186–193, 2004
34. Cebotaru L, Cebotaru V, Wang H, Arend LJ, Guggino WB: STIM1/flKsp-Cre mouse has impaired renal water balance. *Cell Physiol Biochem* 39: 172–182, 2016
35. Igarashi P, Shashikant CS, Thomson RB, Whyte DA, Liu-Chen S, Ruddle FH, et al.: Ksp-cadherin gene promoter. II. Kidney-specific activity in transgenic mice. *Am J Physiol* 277: F599–F610, 1999
36. Isermann B, Hendrickson SB, Zogg M, Wing M, Cumiskey M, Kisannuki YY, et al.: Endothelium-specific loss of murine thrombomodulin disrupts the protein C anticoagulant pathway and causes juvenile-onset thrombosis. *J Clin Invest* 108: 537–546, 2001
37. Traykova-Brauch M, Schönig K, Greiner O, Miloud T, Jauch A, Bode M, et al.: An efficient and versatile system for acute and chronic modulation of renal tubular function in transgenic mice. *Nat Med* 14: 979–984, 2008
38. Worthley LI, Guerin M, Pain RW: For calculating osmolality, the simplest formula is the best. *Anaesth Intensive Care* 15: 199–202, 1987
39. Scarfe L, Schock-Kusch D, Ressel L, Friedemann J, Shulhevich Y, Murray P, et al.: Transdermal measurement of glomerular filtration rate in mice. *J Vis Exp* (140): 58520, 2018
40. Schreiber A, Shulhevich Y, Geraci S, Hesser J, Stsepankou D, Neudecker S, et al.: Transcutaneous measurement of renal function in conscious mice. *Am J Physiol Renal Physiol* 303: F783–F788, 2012
41. Chen L, Chou CL, Knepper MA: A comprehensive map of mRNAs and their isoforms across all 14 renal tubule segments of mouse. *J Am Soc Nephrol* 32: 897–912, 2021
42. Li P, Hu M, Wang C, Feng X, Zhao Z, Yang Y, et al.: LRRC8 family proteins within lysosomes regulate cellular osmoregulation and enhance cell survival to multiple physiological stresses. *Proc Natl Acad Sci U S A* 117: 29155–29165, 2020
43. Lenk GM, Park YN, Lemons R, Flynn E, Plank M, Frei CM, et al.: CRISPR knockout screen implicates three genes in lysosome function. *Sci Rep* 9: 9609, 2019
44. Kumar L, Chou J, Yee CS, Borzutzky A, Vollmann EH, von Andrian UH, et al.: Leucine-rich repeat containing 8A (LRRC8A) is essential for T lymphocyte development and function. *J Exp Med* 211: 929–942, 2014
45. Leheste JR, Melsen F, Wellner M, Jansen P, Schlichting U, Renner-Müller I, et al.: Hypocalcemia and osteopathy in mice with kidney-specific megalin gene defect. *FASEB J* 17: 247–249, 2003
46. Wartosch L, Fuhrmann JC, Schweizer M, Stauber T, Jentsch TJ: Lysosomal degradation of endocytosed proteins depends on the chloride transport protein CIC-7. *FASEB J* 23: 4056–4068, 2009
47. Piwon N, Günther W, Schwake M, Bösl MR, Jentsch TJ: CIC-5 Cl<sup>-</sup> channel disruption impairs endocytosis in a mouse model for Dent's disease. *Nature* 408: 369–373, 2000
48. Castrop H: The role of renal interstitial cells in proximal tubular regeneration. *Nephron* 141: 265–272, 2019
49. Davey MG, Hynes SO, Kerin MJ, Miller N, Lowery AJ: Ki-67 as a prognostic biomarker in invasive breast cancer. *Cancers (Basel)* 13: 4455, 2021
50. Hussy N, Deleuze C, Desarménien MG, Moos FC: Osmotic regulation of neuronal activity: A new role for taurine and glial cells in a hypothalamic neuroendocrine structure. *Prog Neurobiol* 62: 113–134, 2000
51. Boyles JK, Pitas RE, Wilson E, Mahley RW, Taylor JM: Apolipoprotein E associated with astrocytic glia of the central nervous system and with nonmyelinating glia of the peripheral nervous system. *J Clin Invest* 76: 1501–1513, 1985
52. Morgenthaler NG, Struck J, Jochberger S, Dünser MW: Copeptin: Clinical use of a new biomarker. *Trends Endocrinol Metab* 19: 43–49, 2008
53. Olesen ET, Fenton RA: Aquaporin-2 membrane targeting: Still a conundrum. *Am J Physiol Renal Physiol* 312: F744–F747, 2017
54. Sands JM, Layton HE: The physiology of urinary concentration: An update. *Semin Nephrol* 29: 178–195, 2009
55. Shao X, Somlo S, Igarashi P: Epithelial-specific Cre/lox recombination in the developing kidney and genitourinary tract. *J Am Soc Nephrol* 13: 1837–1846, 2002
56. Rickheit G, Wartosch L, Schaffer S, Stobrawa SM, Novarino G, Weinert S, et al.: Role of CIC-5 in renal endocytosis is unique among CIC exchangers and does not require PY-motif-dependent ubiquitylation. *J Biol Chem* 285: 17595–17603, 2010
57. Morris ZS, McClatchey AI: Aberrant epithelial morphology and persistent epidermal growth factor receptor signaling in a mouse model of renal carcinoma. *Proc Natl Acad Sci U S A* 106: 9767–9772, 2009
58. Gaitán-Peñas H, Gradogna A, Laparra-Cuervo L, Solsona C, Fernández-Dueñas V, Barrallo-Gimeno A, et al.: Investigation of LRRC8-mediated volume-regulated anion currents in *Xenopus* oocytes. *Biophys J* 111: 1429–1443, 2016
59. Schober AL, Wilson CS, Mongin AA: Molecular composition and heterogeneity of the LRRC8-containing swelling-activated osmolyte channels in primary rat astrocytes. *J Physiol* 595: 6939–6951, 2017
60. Manolopoulos VG, Liekens S, Koolwijk P, Voets T, Peters E, Droogmans G, et al.: Inhibition of angiogenesis by blockers of volume-regulated anion channels. *Gen Pharmacol* 34: 107–116, 2000
61. Beck FX, Schmolke M, Guder WG, Dörge A, Thurau K: Osmolytes in renal medulla during rapid changes in papillary tonicity. *Am J Physiol* 262: F849–F856, 1992
62. Boettger T, Rust MB, Maier H, Seidenbecher T, Schweizer M, Keating DJ, et al.: Loss of K-Cl co-transporter KCC3 causes deafness, neurodegeneration and reduced seizure threshold. *EMBO J* 22: 5422–5434, 2003
63. Aronson PS, Giebisch G: Mechanisms of chloride transport in the proximal tubule. *Am J Physiol* 273: F179–F192, 1997
64. Planelles G: Chloride transport in the renal proximal tubule. *Pflugers Arch* 448: 561–570, 2004
65. Nilius B, Prenen J, Droogmans G: Modulation of volume-regulated anion channels by extra- and intracellular pH. *Pflugers Arch* 436: 742–748, 1998
66. Igarashi T, Inatomi J, Sekine T, Cha SH, Kanai Y, Kunimi M, et al.: Mutations in SLC4A4 cause permanent isolated proximal renal tubular acidosis with ocular abnormalities. *Nat Genet* 23: 264–266, 1999
67. Gawenis LR, Bradford EM, Prasad V, Lorenz JN, Simpson JE, Clarke LL, et al.: Colonic anion secretory defects and metabolic acidosis in mice lacking the NBC1 Na<sup>+</sup>/HCO<sub>3</sub><sup>-</sup> cotransporter. *J Biol Chem* 282: 9042–9052, 2007
68. Lee HW, Osis G, Harris AN, Fang L, Romero MF, Handlogten ME, et al.: NBCe1-A regulates proximal tubule ammonia metabolism under basal conditions and in response to metabolic acidosis. *J Am Soc Nephrol* 29: 1182–1197, 2018
69. Friard J, Corinus A, Cougnon M, Tauc M, Pisani DF, Duranton C, et al.: LRRC8/VRAC channels exhibit a noncanonical permeability to glutathione, which modulates epithelial-to-mesenchymal transition (EMT). *Cell Death Dis* 10: 925, 2019
70. Ying L, Ma X, Yin J, Wang Y, He X, Peng J, et al.: The metabolism and transport of 1,5-anhydroglucitol in cells. *Acta Diabetol* 55: 279–286, 2018
71. Foreman JW: Fanconi syndrome. *Pediatr Clin North Am* 66: 159–167, 2019

72. Klootwijk ED, Reichold M, Unwin RJ, Kleta R, Warth R, Bockenbauer D: Renal Fanconi syndrome: Taking a proximal look at the nephron. *Nephrol Dial Transplant* 30: 1456–1460, 2015
73. Nielsen R, Christensen EI, Birn H: Megalin and cubilin in proximal tubule protein reabsorption: From experimental models to human disease. *Kidney Int* 89: 58–67, 2016
74. Ma T, Yang B, Gillespie A, Carlson EJ, Epstein CJ, Verkman AS: Severely impaired urinary concentrating ability in transgenic mice lacking aquaporin-1 water channels. *J Biol Chem* 273: 4296–4299, 1998
75. Schnermann J, Chou CL, Ma T, Traynor T, Knepper MA, Verkman AS: Defective proximal tubular fluid reabsorption in transgenic aquaporin-1 null mice. *Proc Natl Acad Sci U S A* 95: 9660–9664, 1998
76. Nilius B: Is the volume-regulated anion channel VRAC a “water-permeable” channel? *Neurochem Res* 29: 3–8, 2004